Original Research

Effect of Cadmium Content on the Properties of Thermally Evaporated $Cu_2(Cd,Zn)SnS_4$ Thin Films and their Solar Cells Performance

Hanaa I.Mohammed [1], Iqbal S. Naji [2], Eman M.Nasir [2,*]

[1] Department of Physics, College of Education for Pure Science (Ibn al-Haitham), University of Baghdad, Baghdad 10071, Iraq.
[2] Department of Physics, College of Science, University of Baghdad, P.O. Box 4732, Baghdad 10071, Iraq.
* Correspondence: eman.nasir@sc.uobaghdad.edu.iq

Received: February 15, 2026; Accepted: May 11, 2026

Abstract: To improve the efficiency of CZTS-based solar cells, it is essential to address the limitations of these systems, such as structural defects, non-ideal band alignment, and high recombination rates. The incorporation of cadmium (Cd) into the CZTS structure is an effective approach to overcome these limitations. In this research, we investigated the effect of Cd content (x = 0.0, 0.5, and 1.0) on the structural, optical, and electrical properties of thermally evaporated thin $Cu_2Cd_xZn_{1-x}SnS_4$ films, which were synthesized from their fabricated alloys. The elemental stoichiometry of CCZTS alloys was verified using EDX analysis. The XRD patterns of CCZTS alloys and thin films confirm the presence of a pure tetragonal phase along the [112] direction. AFM analysis indicated the formation of nanograins in the thin films' structure, and the grain size increased with increasing x-value. The results of UV/Vis spectroscopy revealed that the incorporation of Cd in the prepared thin films resulted in a reduction in the direct allowed band gap from 1.52 eV to 1.38 eV as the cadmium content increased from 0.1- 0.3, respectively. This trend suggests that the incorporation of cadmium affects the electronic band structure of the films, potentially by introducing additional states within the band gap or modifying the band edge. The optical energy gap is a key parameter for photovoltaic applications because it controls the photon energy that the material can absorb. Hall effect measurements showed that all CZTS thin films adopted p-type conductivity, meaning that holes are the majority carriers in these films. The introduction of cadmium did not alter the type of conductivity but increased the holes mobility of in proportion to the cadmium content. These outcomes positively affected the performance of the fabricated CCZTS-based HJ solar cells as their power conversion efficiency increased with increasing Cd content.

Keywords: Cd content; CCZTS thin films; CCZTS-based solar cells; nano-grains; solar cell efficiency

1. Introduction

Second-generation photovoltaic cells, based on the polycrystalline thin Cu (In, Ga)Se_2 (CIGS) and CdTe films, have attracted significant attention due to their good stability and high efficiency, exceeding 18% [1-3]. To increase the market share of solar energy, it is necessary to minimize the production costs and enhance the photovoltaic cells' efficiency. However, potential environmental risks and the scarcity of elements such as Te, In, Ga, and Se create significant challenges to the large-scale production of these technologies [4, 5]. As a result, a thorough study was carried out to identify alternative materials based on cost-effective, non-toxic, and earth-abundant elements, such as Zn and Sn [6-8]. The copper zinc tin chalcogenide compound Cu_2ZnSnS_4 (CZTS) is a promising

candidate to replace the CIGS material. Furthermore, CZTS semiconductor material has become of great interest due to high absorption coefficient ($\alpha > 10^4$ cm^{-1}), which is comparable to that of CIGS, its ideal direct optical energy band gap (1.45-1.6 eV), environmental friendliness, low thermal conductivity, and intrinsic p-type conductivity [6, 9-11]. The Copper zinc tin sulfide quaternary compound is basically derived from the chalcopyrite-type ternary semiconductor compound $CuInSe_2$ (CIS) by substituting half of the indium atoms with zinc and the other half with tin. This process creates a new material with quite similar characteristics to the original compound, but with less expensive and/or rare elements [12, 13], see Fig.1 [14]. Cu_2ZnSnS_4 compounds can crystallize into two main structures: kesterite and stannite. Both structures are tetragonal and feature a cubic close-packed arrangement of sulfur anions, with copper, zinc, and tin cations occupying half of the tetrahedral voids. The stacking sequence is similar to that of zinc blende. The primary distinction between the two structures lies in the arrangement of the cation sublattice. In the kesterite structure, the cationic layers of CuSn, CuZn, CuSn, and CuZn vary with the relative crystallographic coordinate z = 0, 1/4, 1/2, and 3/4, respectively, while in the stannate structure, the layers of ZnS vary with the layers of Cu_2. In both structures, tin and sulfur ions occupy similar lattice positions [12-18]. Many techniques, like spray pyrolysis, spin coating, sputtering, dip coating, SILAR, sol-gel, chemical bath deposition, and thermal evaporation, have been used to fabricate thin CZTS films [19-22]. Solar cells based on thin CZTS films have gained important consideration as an active approach for sustainable thin film photovoltaics. Peksu et al. [23] and Kumar et al. [24] reported that the power conversion efficiency (PCE) of the thermally evaporated CZTS based solar cell was 0.16% and 0.66%, respectively. However, the best experimental efficiency of a single-junction CZTS photovoltaic cell (13%) [11] is much lower than the predicted theoretical efficiency (32%) [25], mainly affected by the significant open-circuit voltage (V_{OC}) lack [26], resulting from charge loss due to non- radiative recombination related to bulk and junction interface defects. To solve these problems, CZTS absorber layers are alloyed with metal elements such as Na, Ag, Co, Cd, and Fe [27-31]. Among these elements, Cd could be a more suitable incorporation element for CZTS to create $Cu_2(Cd_xZn_{1-x})SnS4$ (CCZTS)[32]. Cd alloying adjusts the band gap and electronic structure besides suppressing undesirable secondary phases, offering a promising path to improve kesterite thin films for high-efficiency photovoltaic applications [33]. Z.Su et al. [34-36] prepared CCZTS thin films using the spin-coating technique from their precursor solution prepared by the sol-gel method. As a result, the PCE of the fabricated (glass/Mo/Cu_2(Cd, Zn)SnS_4/CdS/ITO) photovoltaic cells was increased from 5.1% for pure CZTS to 12.6% for Cu2Cd0.4Zn0.6SnS4. A previous study showed an increase in the power conversion efficiency (PCE) from 5.3% for Cu2ZnSnS4 to over 11% for $Zn_{0.6}Cd_{0.4}SnS_4$, and reached 8.11 for $Cu_2ZnSn(S, Se)_4$ at a Cd/(Cd+Zn) content of 5% [33]. Wang et al. [37] adopted a nanoparticle ink method to prepare Cu_2 (Cd, Zn)SnS_4 thin films. Because of their comparatively excellent crystallization and photoresponse properties, the highest PCE of 0.72 was obtained at a Cd/Cd+ Zn= 0.3 for manufactured glass / CCZTS / CdS / ZnO / ITO / Ag single heterojunction solar cells. To prepare thin Cu_2(Cd, Zn)SnS_4 films, Yan et al. [38] adopted the chemical bath deposition (CBD) technique to deposit CdS (Cd source) onto the co-sputtered Cu/ZnS /SnS structure. The alloying of Cd was found to significantly affect the CCZTS electrical properties, the microstructure, secondary phases, the alignment of energy bands at the CCZTS/buffer interface, and the band tailing. The fabricated photovoltaic cell based on $Cu_2Cd_{0.4}Zn_{0.6}SnS_4$ achieved an

efficiency exceeding 11%. Thin CCZTS films with different Cd gradients were successfully prepared by Wang et al. [32] using the nanoparticle ink technique. The incorporation of Cd in CZTS films, modulates the energy band gap, and enhances the film crystallinity. The PCE of the fabricated CCZTS thin film solar cell reached 5.61 %. Conversely, several theoretical results have indicated the potential of enhancing the performance of CZTS-based PV cells by modifying the characteristics of various layers and controlling the used substances. A recent study showed that modifying the optical energy band gap of the Zn:Al window layer to 3.5 eV improves the efficiency of the MoS_2/p-CZTS/n-ZnS/i-ZnO/n-ZnO:Al solar cell to 29.1%, whereas the solar cell performance reached 28.9% when the energy band gap of the CZTS absorber layer was increased to 1.35 eV [39]. Mazumder et al. [40] designed and simulated the bilayer structures (pp+) for CZTS photovoltaic cells along with analyzed the role of front and back contact metal work function, shunt and series resistance, CZTS (p)/CZTS (p+) layer thickness, and the energy band gap in obtaining the highest power conversion efficiency of 20.34%. Bouarissa et al. [41] suggest a design of a ZnO/MoS_2/CZTS solar cell where MoS_2 reformed the classical buffer layer (CdS) and examined the impacts of the doping ratios and the thickness of the design on the electrical parameters of the proposed CZTS-based PV cell with high power conversion efficiency of 23.69%. To enhance the efficiency of the CCZTS-based single-junction photovoltaic cell, a tandem solar cell is a suitable option. This could be linked with the variation of band gap energies of different materials which can, hopefully, cover the whole wavelength range of the solar spectrum. High energy band gap thin film photovoltaic cells, including chalcopyrite, III-V, perovskite, and kesterite, have received great attention due to their possibility applications as a top cell in tandem solar cells and as single-junction photovoltaic devices [42]. Substituting Cu^+, Zn^{2+}, or Sn^{4+} in CZTS with Ag^+, Ba^{2+}, or Ge^{4+}, respectively, allows for acceptable tuning of its energy band gap, its lattice parameters, and its imperfections, making it appropriate for new applications, such as indoor photovoltaic (IPVS) and tandem structures, that required wider band gaps [43]. Gong et al. [44] demonstrated that replacing Cu^+ with Ag+ in CZTS $(Ag_xCu_{1-x})_2ZnSnS_4$ could modify the band gap from 1.5 to 2.0 eV, while Mengü et al.[45] reported that introducing Ge^{+4} into CZTS $(Cu_2Zn(Sn_{1-x}Ge_x))S_4$ adjusts the band gap from 1.5 to 2.25 eV. A CZTS/CZTSSe tandem photovoltaic cell with 1 eV CZTSSe-based lower subcell and 1.3 eV CZTS-based upper subcell was designed and optimized (500 nm CZTSSe, 900 nm CZTS) to attain a maximum power conversion efficiency of 38.21% [46]. In another theoretical investigation carried out by Ennouhi et al. [47], the performance of a kesterite/c-Si tandem solar cell was boosted by using a TiO_2 buffer layer instead of CdS in the kesterite top subcell. The kesterite/TiO_2 tandem cell achieved higher performance (20.18%) than kesterite/CdS (16.5%) due to the enhancement of optical properties and a reduction in recombination rates.

Despite significant progress in the preparation of $Cu_2Cd_xZn_{1-x}SnS_4$ thin films using chemical techniques and multi-stage methods in recent years and the good control these methods provide over prepared thin films' composition and properties, the direct preparation of these films using the vacuum thermal evaporation (VTE) technique from a pre-synthesized alloy as a single evaporation target has received little interest in the scientific literature. This deficiency of attention is attributed to the challenges associated with the different vapor pressures of the constituent elements, which can lead to deviations in the chemical composition of the deposited films. However, the VTE

method is characterized by its simplicity, inexpensiveness, and industrial suitability. Furthermore, the prepared thin films adopt high purity, high adhesion, and good homogeneity.

Therefore, this study aims to prepare $Cu_2Cd_xZn_{1-x}SnS_4$ thin films from their pre-fabricated alloys using the vacuum thermal evaporation route and evaluates the influence of Cd content (0.0, 0.5, and 1.0) on the structural and optoelectronic properties of $Cu_2Cd_xZn_{1-x}SnS_4$ thin films. In addition, investigate how these characteristics impact the photovoltaic cell performance.

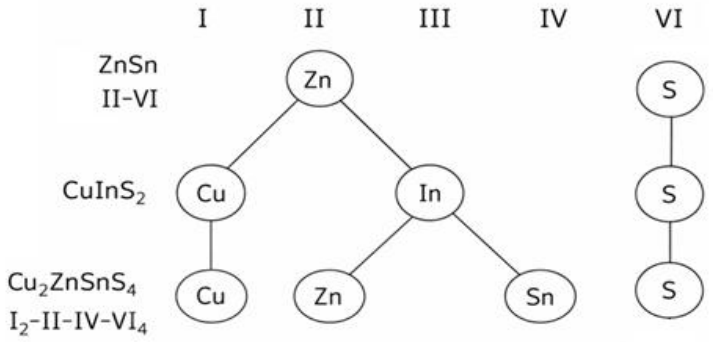

Figure 1. Cross-replacement stages to produce I_2-II-IV-VI_4 compound [14].

2. Materials and methods

To fabricate Cu_2(Cd, Zn)SnS_4 alloys with various Cd contents (0.0, 0.5, and 1.0), suitable amounts of the constituent elements with a purity of 99.999% were employed. The elements were well mixed and then placed in clean, dry quartz tubes, each of 15 cm in long, which were evacuated to 10^{-2} mbar. The quartz tubes were then positioned in a programmable Carbolite electric furnace. To ensure thorough mixing and homogeneity during melting, the tubes were fixed at an angle of 45°. The temperature of the furnace was gradually increased at a constant rate of 3 K/min until it reached 1173 K. The temperature was fixed at 1173 K for 2 hours. Then, the furnace was turned off, and the samples were kept inside the furnace to cool down slowly up to room temperature. After cooling, the ingots were removed from the quartz tubes, finely grounded, and stored in glass containers as shown in Figure 2. The resulted materials were then used to deposit CCZTS thin films at room temperature on pre-cleaned single-crystal silicon and glass substrates. In solid substances, the crystallization process is mainly depended on atomic movement within the crystalline lattice, which is controlled by activation energy (Ea) and the diffusion temperature (T). The coefficient of atomic diffusion (D) increases with increasing the diffusion temperature, follow the Arrhenius formula: $D = D_0 \exp\left[\frac{-E_a}{k_B T}\right]$, where D_0 is the pre-exponential diffusion factor, and k_B is the Boltzmann constant [48, 49]. Higher temperatures improve the atomic motion and facilitating the atomic migration to their correct lattice sites, thus enhancing crystalline growth and the creation of a homogeneous crystal phase. At lower temperatures, the energy provided to the atoms is insufficient to climb the energy barriers, resulting in slowing down the solid–solid reactions, decreasing the atomic rearrangement, delaying the crystalline growth, and a higher probability of developing undesirable phases [48, 49]. On the other hand, at extremely high temperatures, intense movement of atoms can cause the loss of volatile constituent elements or chemical instability, negatively impacting the stability of the crystal phase [48-50]. For this reason, the crystallization temperature is accurately chosen for achieving a balance between supplying the requisite atomic movement for the crystalline lattice reorganization and boosting regulated crystal growth, while

simultaneously securing the solid state thermodynamic. The vacuum thermal evaporation method under a vacuum of 10^{-5} torr was used to deposit the thin films with a 600 nm thickness and a deposition rate of 0.83 nm/sec.

The elemental composition of all prepared alloys was verified using an Energy Dispersive X-ray Spectrometer (EDS) type AIS 2300C.

X-ray diffraction (XRD) information of the fabricated samples (alloys and their thin films) was obtained via an X-ray diffractometer, Shimadzu-Japan-XRD 6000, supplied with a Cu Kα radiation of 1.541 Å wavelength (λ). The inter-planar distances $d(hkl)$ for diverse planes were estimated by applying Bragg's law [51]:

$$2dsin\theta = n\lambda \quad (1)$$

Where θ is the diffraction angle and n is the reflection order (n=1).

The average crystallite size (D) of the CCZTS structures was determined from the full width at half maximum (FWHM) (B) of the prominent peak using the Debye-Scherrer equation [51]:

$$D = \frac{0.94\lambda}{Bcos\theta} \quad (2)$$

Furthermore, the lattice constants (a and c) were calculated by the following relationship [52]:

$$\frac{1}{d^2} = \frac{h^2 + k^2}{a^2} + \frac{l^2}{c^2} \quad (3)$$

And the volume of the unit cell was determined from the equation below [53]:

$$V = a^2c \quad (4)$$

Also, lattice defects, dislocation density (δ), and microstrain (ε) were estimated using the following formulas [54]:

$$\delta = 1/D^2 \quad (5)$$

$$\varepsilon = Bcos\theta/4 \quad (6)$$

The surface morphology of all prepared thin films was examined by atomic force microscopy (AFM) in contact mode with a silicon tip (scanning probe microscopy type AA3000).

To investigate the optical characteristics of thin CZTS films, the transmittance (T) and absorption (A) spectra of the examined samples were recorded by the UV-Vis-NIR spectroscopy in the wavelength range of 350 - 1100 nm.

The absorption coefficient (α) was calculated using the formula shown below [55,56]:

$$\alpha = \frac{2.303A}{t} \quad (7)$$

Where t is the thickness of CCZTS thin films.

The thickness of the thin films was measured using the gravimetric approach, as expressed in the formula [57]:

$$t = \Delta m/A\,\rho \quad (8)$$

Where Δm is the difference in glass substrate weight before and after deposition, A is the sample area, and ρ is the density of the deposited thin film material.

The optical energy band gap (E_g^{opt}) of thin $Cu_2(Cd, Zn)SnS_4$ films was estimated graphically using the Tauc equation [52]:

$$\alpha h\upsilon = \beta\left(h\upsilon - E_g^{opt}\right)^r \quad (9)$$

Where β is a constant inversely proportional to amorphousness, $h\nu$ represents the photon energy, and r is the exponential factor dependent on the type of transition.

The extinction coefficient (k) can be determined using the following relationship [58]:

$$k = \alpha\lambda/4\pi \tag{10}$$

The optical conductivity of CCZTS thin films was measured using the formula below [59]:

$$\sigma_{opt.} = \alpha nc/4\pi \tag{(11)}$$

Where n is the refractive index of the thin films and c is the speed of light.

The Hall effect measurement system was employed to estimate the electrical characteristics of the deposited CCZTS thin films, which included carrier concentration (P), Hall coefficient (R_H), Hall mobility (μ_H), Hall resistivity (ρ_H), and Hall conductivity (σ_H). These characteristics were calculated using the equations shown below [60]:

$$P_H = 1/e.R_H \tag{12}$$

Where e is the electron's charge.

$$R_H = \frac{slope * t}{B_Z} = \frac{\frac{V_H}{I_x} * t}{B_Z} \tag{13}$$

Where B_Z is the applied magnetic field, V_H is the electric potential difference across the sample, and I_x is the current passing through the sample.

To calculate the power conversion efficiency (PCE) of Al/p-CCZTS/n-Si/Al solar cells, current and voltage measurements were performed under dark conditions and during illumination (air mass 1.5 with incoming power density (P_{in} =100 mW/cm²). The following parameters were evaluated: short circuit current (I_{sc}), open circuit voltage (V_{oc}), fill factor ($F.F.$), maximum power (P_m), and conversion efficiency (η). The fill factor and conversion efficiency were calculated using standard equations [61]:

$$F.F = \frac{P_{max}}{V_{oc}I_{sc}} = \frac{V_{max}I_{max}}{V_{oc}I_{sc}} \tag{14}$$

$$\eta = \frac{P_{max}}{P_{in}} * 100\% = \frac{F.FV_{oc}I_{sc}}{P_{in}} * 100\% \tag{15}$$

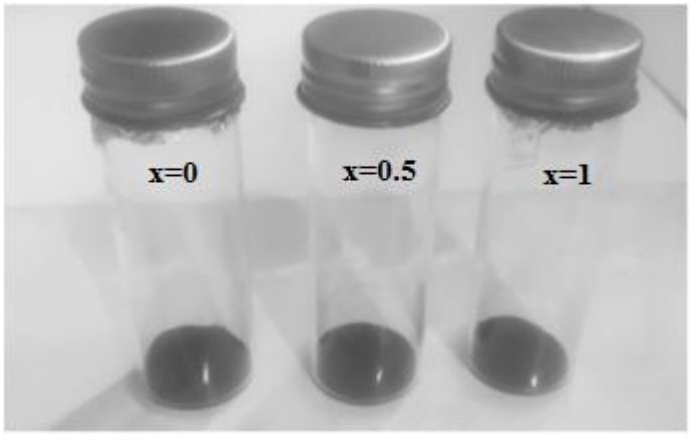

Figure 2. $Cu_2CdxZn_{1-x}SnS_4$ powders of prepared alloys

2. Results and discussions

The measured atomic ratios of the prepared alloys are shown in Table 1. The obtained values of Cd/(Cd+Zn) were close to the theoretical values, while the measured Sn/(Cd+Zn) ratios were lower than the theoretical values. This is attributed to the volatilization of tin (Sn) during the heat treatment in the preparation of the alloys. The atomic ratios of Cu/(Cd+Zn) were less than 2, indicating that CCZTS alloys show copper deficiency [37], and the thin films are likely to be copper poor as well. It is well-established that solar cells based on thin Cu-poor films are expected to achieve high efficiency [62]. The energy dispersive X-ray (EDX) spectra of CCZTS alloys (Figure 3) reveal that the fabricated alloys consist only of their constituent elements, without additional elements detected in the alloy powders, confirming the high purity of the prepared samples. In addition, the absence of an oxygen peak indicates that the alloys were manufactured in a completely oxygen-free atmosphere.

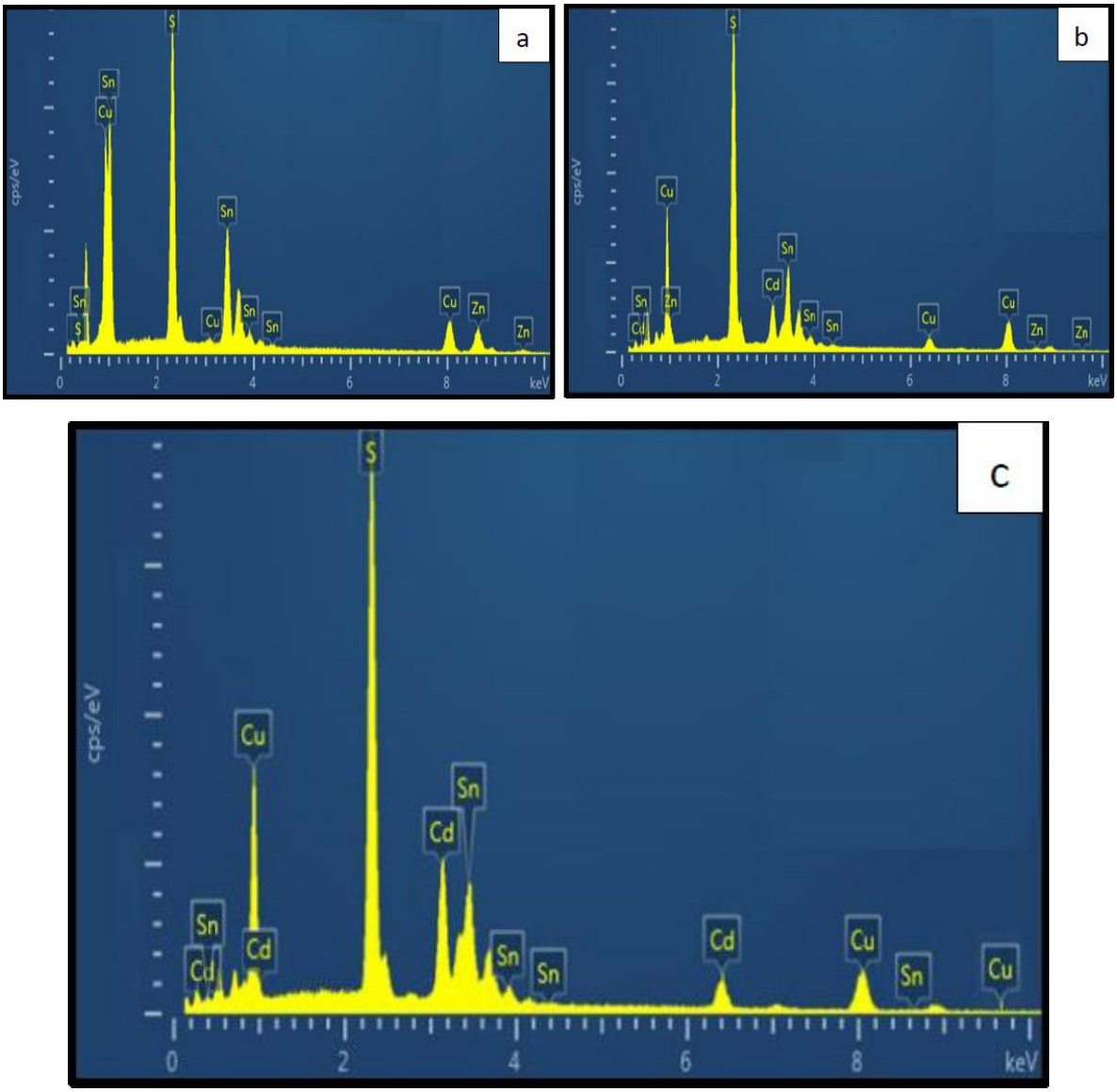

Figure 3. EDXA spectra of $Cu_2CdxZn_{1-x}SnS_4$ alloys for (a) x=0.0, (b) x=0.5, and (c) x=1.0

Table 1. Atomic ratios of $Cu_2(CdxZn_{1-x})SnS_4$ alloys.

Atomic Ratios			
Cu/(Cd+Zn)	**Sn/((Cd+Zn)**	**Cd/(Cd+Zn)**	**Samples**
1.94	0.91	0	**Cu_2ZnSnS_4**
1.62	0.97	0.48	**$Cu_2Cd_{0.5}Zn_{0.5}SnS_4$**
1.53	0.98	0.97	**Cu_2CdSnS_4**

XRD analysis was employed to examine the changes in crystal phases of $Cu_2Cd_xZn_{1-x}SnS_4$ nanocrystals (CCZTS NCs) alloys and thin films as Zn is substituted by Cd. The XRD results (Figure 4, a and b) reveal a phase transition from the tetragonal kesterite (KS) of $Cu_2Cd_xZn_{1-x}SnS_4$ NCs, with x = 0 and 0.5 (JCPDS No. 26-575 for CZTS), to the tetragonal stannite (ST) of Cu_2CdSnS_4 NCs (x = 1) (JCPDS No. 26-506). This transformation has been reported by Ibraheam et al. and Rondiya et al. [63, 64]. It is clear from figure 4 and Tables 2a and c that the position of the main diffraction peak (112) shifts to lower 2θ, and this shift increases with increasing Cd content. As observed in previous studies [35, 64], the shift of the (112) plane towards smaller angles confirms the replacement of Zn^{2+} with Cd^{2+}. This indicates that the inter-planar space and the size of the unit cell are increased with increasing cadmium content [53]. This phenomenon occurs because cadmium has a larger ionic radius, 0.80 Å compared to zinc, 0.75 Å [37, 65]. The obtained result aligns-well with previous studies [35, 66]. Furthermore, no additional peaks associated with other phases or impurities were observed in the XRD patterns of any of the fabricated alloys or thin films. The lack of extra peaks in the X-ray diffraction spectra suggests the creation of a single-phase structure within the detection limit of the XRD technique. Nevertheless, the existence of secondary phases in tiny quantities underneath the threshold observation cannot be excluded. However, the EDX results, which indicated the absence of foreign elements related-peaks, together with overall concordance within the chemical composition despite slight deviations such as tin volatilization and copper deficiency, support the deduction of phase purity for all prepared specimens in the sensitivity and accuracy limits of the measurement techniques utilized. This result suggests that the addition of cadmium to the CZTS NC lattice contributed to expanding the single-phase region and preventing the formation of secondary phases. This conclusion is consistent with previous observations [64, 66]. While, Whearse Migdadi et al. [53] reported the existence of peaks in the XRD spectra of pure and Cd-doped with 1%, 2%, and 4% CZTS films, which were attributed to the CZTS kesterite phase and $ZnSO_3$ and CdS secondary phases. This dissimilarity in the results of Ref [53] and those of the present study may be attributed to the differences in the doping ratios and preparation conditions. The lattice constants (a and c) of the CCZTS NC alloys were calculated to be in a good agreement with the standard values, as shown in Table 1a. Another observation suggests that, as the cadmium concentration increases, the full width at half maximum of the main peak decreases, which leads to increase the crystal size. As a result, both dislocation density and microstrain are decreased, as seen in Table 2b and c. This result aligns with the findings of previous studies [63, 66]. The lower values of δ and ε for CCTS NC alloys and thin films indicate fewer imperfections and better stability of the crystal structure.

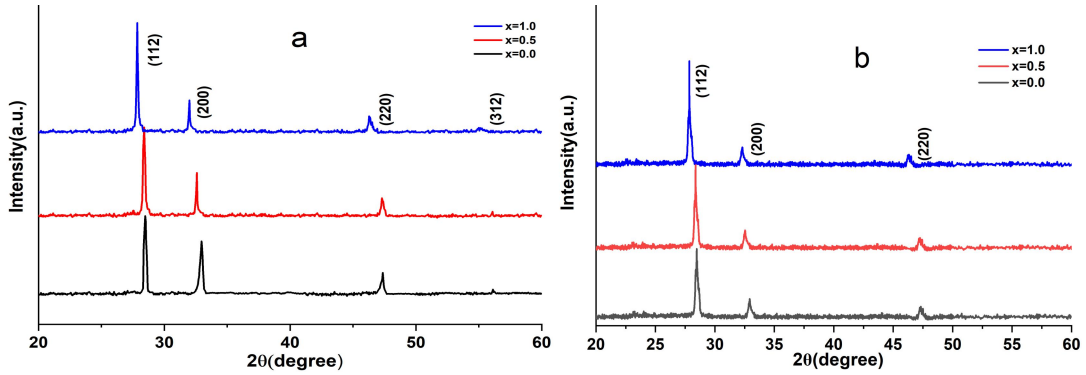

Figure 4. XRD spectra of (a) $Cu_2Cd_xZn_{1-x}SnS_4$ alloys and (b) $Cu_2Cd_xZn_{1-x}SnS_4$ thin films.

Table 2a. Lattice parameters of $Cu_2Cd_xZn_{1-x}SnS_4$ compounds.

***V* (Å^3)**	***a,c* stand. (Å)**	***a,c* exp. (Å)**	***hkl***	**2*θ* (deg.)**	**D_{stand} (Å)**	**d_{exp}(Å)**	***x***
318.6427	*a*=5.427,	*a*=5.431,	112	28.4824	3.126	3.122	0.0
	c =10.848	*c*=10.803	200	32.9398	2.713	2.715	
			220	47.3208	1.919	1.918	
			312	56.1496	1.636	1.636	
321.2100		*a*=5.488,*c*=10.665	112	28.4102	/	3.137	0.5
			200	32.5899	/	2.744	
			220	47.3100	/	1.919	
			312	56.0911	/	1.637	
338.7640	*a*=5.586,*c*=10.834	*a*=5.580,*c*=10.880	112	27.8990	3.192	3.194	1.0
			200	32.0401	2.791	2.790	
			220	46.2800	1.975	1.959	
			312	55.0000	1.679	1.667	

Table 2b. Crystallite size (*D*), dislocation density (*δ*), and microstrain (*ε*) of prepared alloys.

***ε**10^{-4}**	***δ**10^{14} lines/m^2**	***D* (nm)**	**FWHM (deg.)**	***hkl***	***x***
9.6342	7.0868	37.5641	0.2278	112	0.0
8.8828	6.0245	40.7416	0.2100	112	0.5
6.7881	3.5182	53.3136	0.1603	112	1.0

Table 2c. Lattice parameters of thin $Cu_2Cd_xZn_{1-x}SnS_4$ films.

***ε**10^{-3}**	***δ**10^{14} lines/m^2**	***D* (nm)**	**FWHM (deg.)**	***hkl***	**d_{exp} (Å)**	**2*θ* (.deg)**	***x***
1.3310	13.5257	27.1906	0.3147	112	d_{exp}.=3.122	28.4719	0.0
1.3067	13.0371	27.6955	0.3089	112	d_{exp}.=3.137	28.3784	0.5
1.2858	12.6225	28.1466	0.3036	112	d_{exp}.=3.194	27.8530	1.0

The topographical features of the CCZTS thin films are presented in both 2D and 3D images (Figure 5). The 2D AFM micrographs reveal the presence of spherical nanoparticles with some voids distributed across the surfaces of the films. The results showed that a higher cadmium content yielded larger average particle sizes, which reduced the number of surface voids and led to

a denser surface. These findings agree with the reduction in dislocation density and microstrain calculated from XRD results, indicating an improvement in crystalline quality and a decrease in structural defects. Average particle diameters were measured to be 34.19, 45.11, and 55.04 nm for the three Cd contents, respectively. The same trend was observed in the crystallite size, which was estimated from XRD results (Table 1c). This may be related to the nucleation and growth of particles during the crystallization process [67], which is expected to increase with higher cadmium content. This finding is in good agreement with a previous study [32], which indicated that Cd doping of CZTS is necessary for grain growth. To produce high-efficiency solar cells, larger grain sizes are essential. Increasing the grain size reduces the number of grain boundaries, which in turn enhances the effective diffusion length of minority carriers. This results in an increase in the short-circuit photocurrent of polycrystalline solar cells [12, 68]. From the 3D images of the prepared thin films, the sharp and dense pyramidal structures were observed. The mean surface coarseness of the films was evaluated as 0.821, 1.063, and 1.206 nm for all Cd concentrations. This means that surface roughness increases with increasing Cd content. Variations in the surface coarseness of a film can significantly impact its electrical and optical properties, thereby affecting its suitability for various applications. Enhanced surface coarseness leads to increased multiple reflections of photons on the surface, which enhances the probability of photon absorption and, consequently, improves the efficiency of solar cells [69].

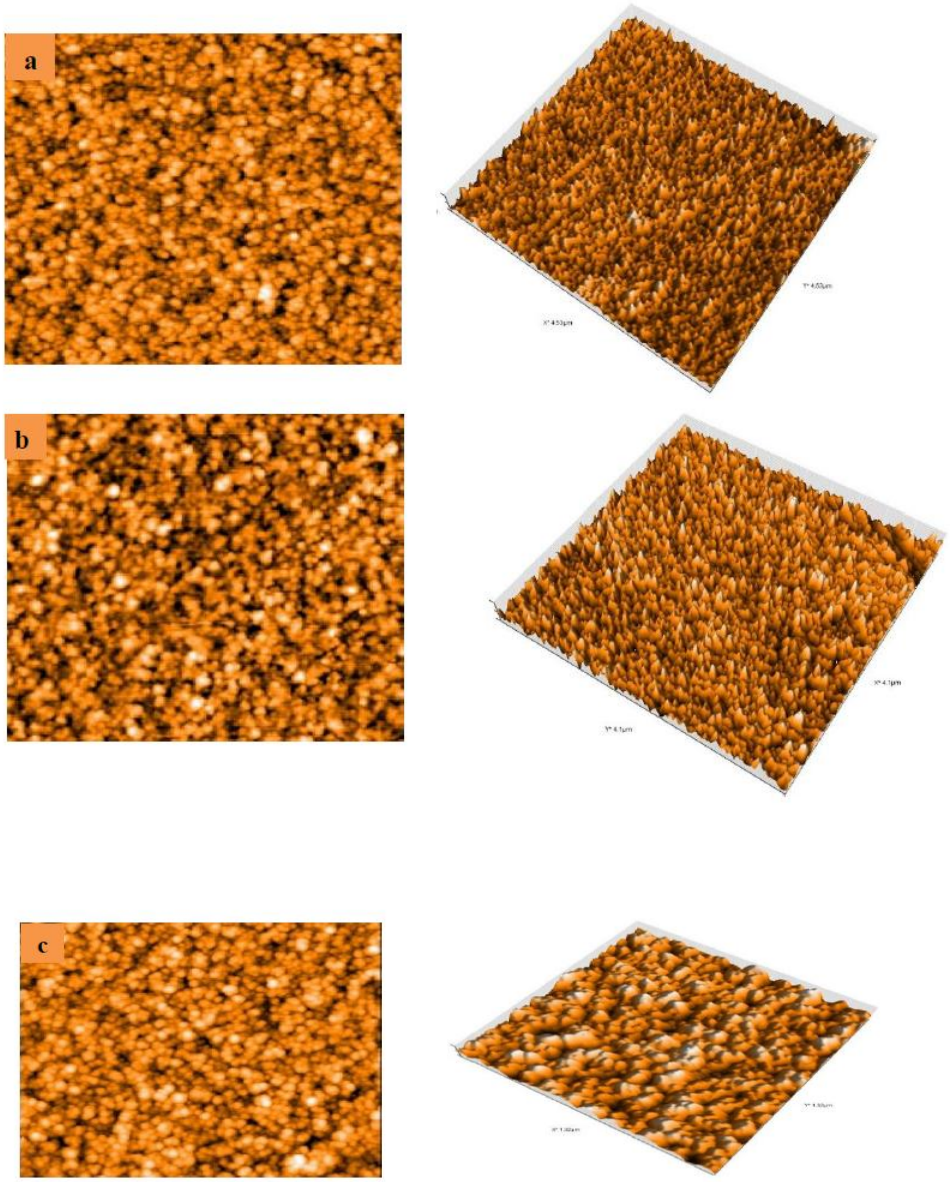

Figure 5. 2D and 3D AFM images of $Cu_2Cd_xZn_{1-x}SnS_4$ thin films for (a) x=0.0, (b) x=0.5, and (c) x=1.0

Figure 6(a) illustrates the absorbance spectra over the wavelength range 350-1100 nm for the pure and Cd alloyed CZTS thin films deposited on glass substrates. It is clear that the absorbance of CCZTS thin films increases with decreasing the wavelengths of incident light and becomes very high and quasi-stable in the ultraviolet to visible region (350-500 nm). This may be attributed to the complete absorption of photons with higher energies than the CCZTS thin-film energy gap. This result was consistent with a previous study [25]. On the other hand, the absorbance of the thin film increases with increasing Cd ratio, which may be related to increase the film's surface roughness [70]. The absorption edge region in Vis-NIR (500- 900nm) is the most essential segment of the figure, where absorbance falls sharply. As can be seen, the absorption edge of the prepared thin films shifts towards lower energies (i.e., longer wavelengths) when the Cd content in the host matrix increased. Over the low energy region (NIR, where wavelengths are longer than 900 nm), incident photons have energy less than the energy band gap of the material; therefore, the material becomes

transparent. Figure 6(b) displays the corresponding transmittance spectra of the fabricated thin films. The transmittance spectra show the opposite behavior to the corresponding absorbance.

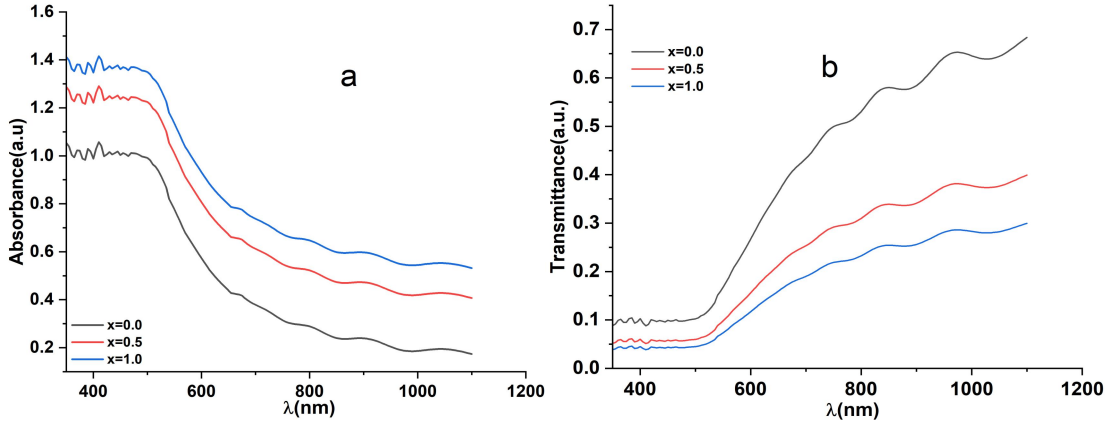

Figure 6. (a) Absorbance and (b) transmittance spectra of thin $Cu_2Cd_xZn_{1-x}SnS_4$ films as a function of wavelength

Another key optical parameter for evaluating the behavior of thermally evaporated CCZTS thin films is the absorption coefficient. As seen in Figure 7, all the prepared thin films exhibit a high absorption coefficient ($\alpha > 10^4$ cm^{-1}), denoting the presence of a direct band gap in the films. This finding is compatible with previous studies [37, 71]. The figure also shows that the absorption coefficient decreases with increasing the wavelength of incident photons, which means that the absorption coefficient increases with increasing incident photon energy. This increase is due to the interaction between the semiconductor's electrons and the photons when the photon energy is sufficient to induce electronic transitions. In addition, the absorption coefficient increases with increasing cadmium content.

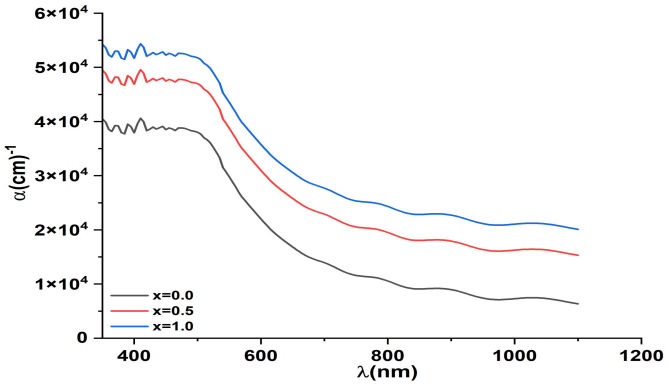

Figure 7. Absorption coefficient of $Cu_2Cd_xZn_{1-x}SnS_4$ thin films as a function of wavelength.

To understand how the cadmium content affects the optical band gap of thin CCZTS films, the Tauc plot was used (Figure 8a-c). The value of the intersection on the graph represents the band gap energy, assuming that the absorption coefficient is equal to zero. The estimated band gap values were 1.52 eV, 1.44 eV, and 1.38 eV for the 0.0, 0.5, and 1.0 Cd concentrations, respectively. The findings revealed that the Eg^{opt} value decreased with increasing Cd concentration; and this narrowing can be attributed to the localized Cd-induced states near the bottom of the conduction band [33]. The decline in the energy band gap can also be clarified by the empirical rule for semiconductors: substituting a heavier element instead of a lighter one in the host structure, which

is from the same group in the periodic table, decreases the energy band gap of the semiconductor compound [72]. This result is consistent with a previous study [73]. The obtained optical band gap values for CZTS and CCTS are close to those reported in previous reports [74, 75]. Rondiya et al .[66] showed that the estimated direct energy band gap of CCZTS thin films decreased from 1.51 eV to 1.03 eV when the Cd content increased from 0 to 1. While Su et al. [35] observed that, when the Cd concentration increased from 0 to 1.0, the direct energy band gaps of CZCTS thin films decreased from 1.54 eV (CZTS) to 1.36 eV (CZCTS) and then increased to 1.41 eV. The variations in the values of calculated energy band gaps indicate that the energy band gap of CCZTS thin films is affected by several parameters, such as grain size, thickness, defects, and elemental composition. In this context, the optical characteristics of CZTS absorber layers can be improved by swapping zinc atoms with cadmium atoms, yielding a lower energy band gap [63]. Finally, we can say that, our results are in agreement with the general direction that alloying metal elements would modify the structure of the band gap (i.e., the electronic characteristics) of the host matrix [76].

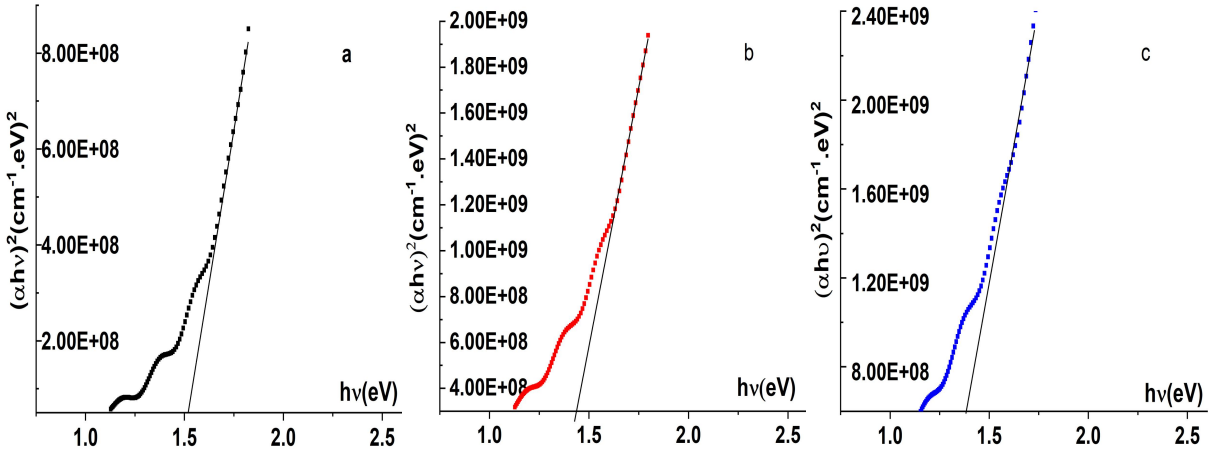

Figure 8. $(\alpha h\nu)^2$ as a function of $(h\nu)$ for thin $Cu_2Cd_xZn_{1-x}SnS_4$ films with different Cd content (a) x=0.0, (b) x=0.5, and (c)x=1.0

Figure 9 shows how the extinction coefficient of CCZTS thin films behaves with the change in cadmium content. The figure clearly shows that the extinction coefficient follows a trend similar to that of absorptance or absorption coefficient, i.e., increase with increasing cadmium content. This is because the extinction coefficient is directly dependent on light absorption, as seen in Eq. (10).

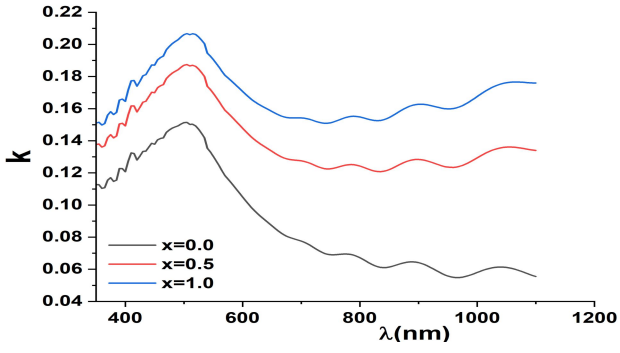

Figure 9. Extinction coefficient of $Cu_2Cd_xZn_{1-x}SnS_4$ samples with different Cd content as a function of wavelength.

Figure 10 shows the variation in the optical conductivity (σ_{opt}) of prepared thin films with cadmium content, where all films showed very high optical conductivity values, and their conductivity increased with increasing cadmium content, which may be attributed to the strong absorption of excited electrons [77].

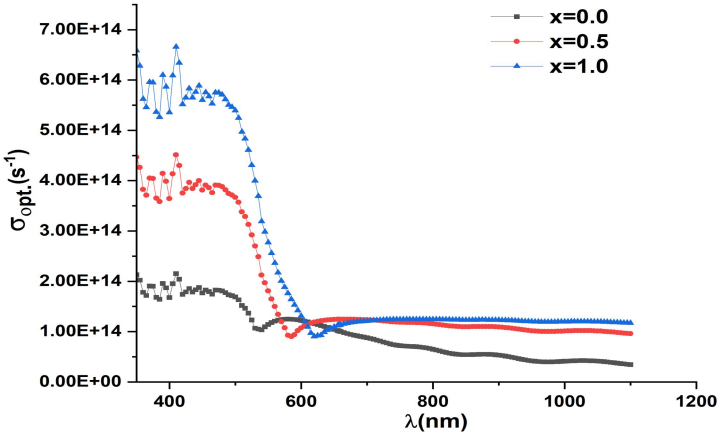

Figure 10. Optical conductivity of $Cu_2Cd_xZn_{1-x}SnS_4$ samples with different Cd content as a function of wavelength.

Table 3. Hall effect measurements results of $Cu_2Cd_xZn_{1-x}SnS_4$ samples.

Carrier Type	Conductivity $(\Omega.cm)^{-1}$	Mobility $(cm^2/V.s)$	Carrier Con.*10^{17} (cm^{-3})	Cd content
p	0.1326	0.0923	89.810	0.0
p	0.0346	0.3312	6.5481	0.5
p	0.0226	0.7528	1.8799	1.0

Table 3 summarizes the electrical transport characteristics of thin CCZTS films. All the prepared samples exhibited p-type conductivity. This result agrees with [63]. The carrier concentration (holes concentration) decreased with higher Cd content, which can result from compensating the intrinsic acceptor lattice defects. Cu_{Zn} antisite defects are the dominant type of acceptor defects in CZTS because of their shallow level and low formation energies [14, 78], therefore, they are responsible for the positive conductivity of CZTS thin films. All prepared thin films adopted a Cu- poor composition, denoting they contained many copper voids (V_{Cu}) that acted as acceptor defects in addition to the Cu_{Zn}. When Cd is incorporated into the CZTS lattice, Cd atoms can replace the metal sites such as Cu, Zn, and Sn. Cd_{Cu} as donor defects can compensate for Cu_{Zn} and V_{cu} [79], which in turn leads to lower holes concentration and weaker conductivity. This result is consistent with [80]. Conversely, with a reduction in holes concentration, their mobility rises, perhaps due to a decline in collisions between holes.

To investigate the influence of Cd substitution on the performance of Al/CCZTS/Si/Al HJ solar cells, photovoltaic measurements were carried out on thin CCZTS films. Fig.11 shows the illuminated current-voltage (I-V) curves for CCZTS absorber layers, while the main photovoltaic parameters are shown in Table 4. From Table 4, the solar cell based on thin CZTS films adopted a lower open-circuit voltage (Voc) and short-circuit current (Isc), which can result from the high

density of defects and grain boundaries in the absorber layer. The power conversion efficiency of fabricated solar cells increased with increasing Cd content. Solar cells based on CCTS thin films (x=1) achieved the highest power conversion efficiency of 2.621%, with corresponding Voc, Isc, and F.F values of 0.651V, 0.0117A, and 0.341, respectively. The presence of a tunable direct energy band gap, a high absorption coefficient, and grain growth in thin Cu_2ZnSnS_4 films by Cd alloying enhances the minority charge carrier's lifetime and diffusion length, thereby decreasing the recombination process and improving charge carrier separation, therefore, increasing the photovoltaic cell efficiency. The disparity in the efficiency magnitudes reported in this study and those calculated in previous studies may be due to the variations in the preparation conditions, solar cell structure, and preparation method.

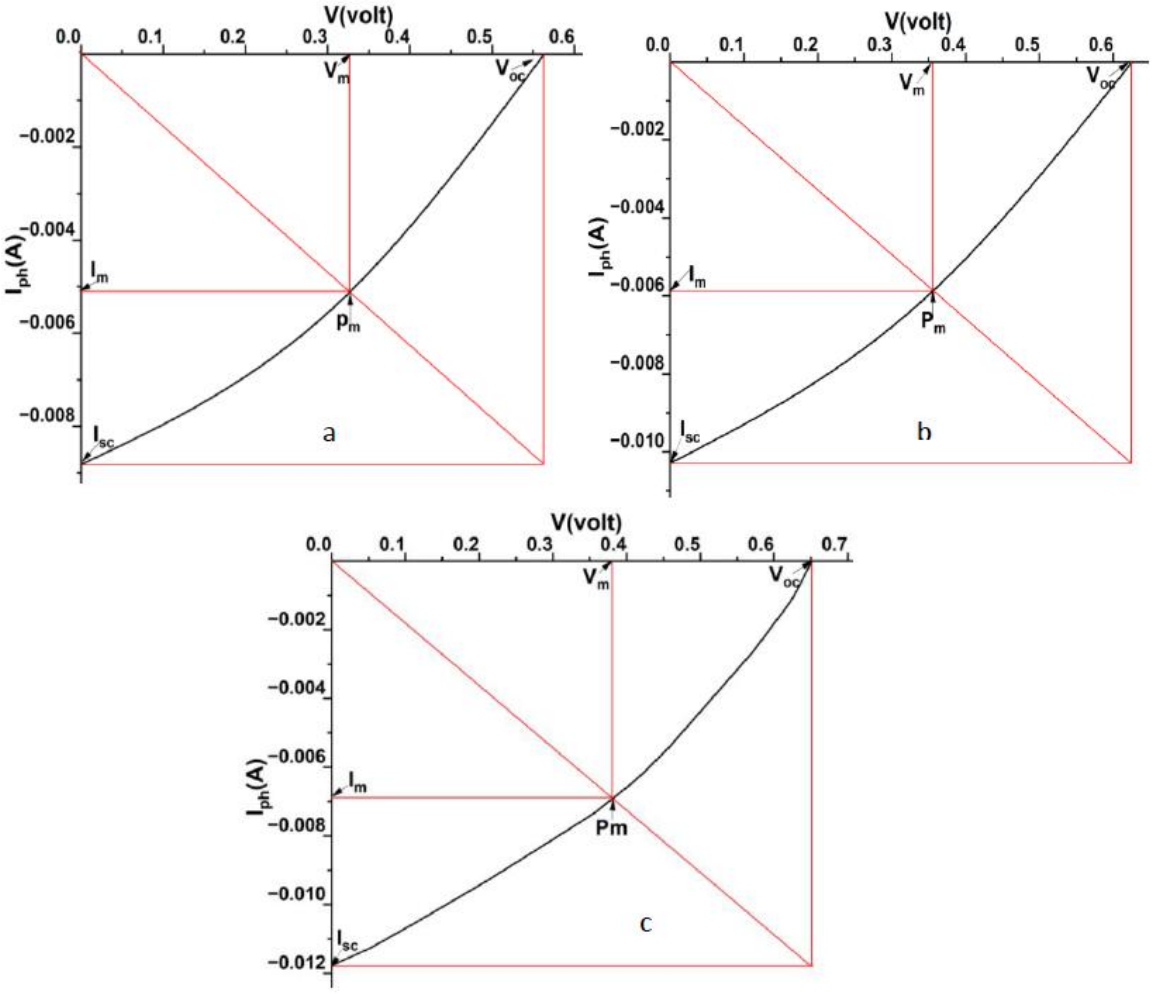

Figure 11. I-V curves of $Cu_2Cd_xZn_{1-x}SnS_4$ / **Si** heterojunction solar cells for (a) x=0.0, (b) x=0.5, and (c) x=1.0

Table 4. Photovoltaic parameters of $Cu_2Cd_xZn_{1-x}SnS_4$ - based solar cells.

η%	*F.F*	V_{OC} (V)	I_{Sc} (A)	V_m (V)	I_m (A)	*x*
1.6637	0.3360	0.5627	0.0088	0.3263	0.0051	0.0
2.0702	0.3250	0.6245	0.0102	0.3570	0.0058	0.5
2.5862	0.3395	0.6511	0.0117	0.3804	0.0068	1.0

4. Conclusions

$Cu_2Cd_xZnxSnS_4$ thin films have been successfully prepared by vacuum thermal evaporation method from pre-fabricated alloys with controlled Cd content of x=0.0, 0.5, and 1.0**.** The insertion of cadmium into CZTS thin films has a pronounced effect on their optical and electronic properties, making CCZTS a suitable absorber for good-efficiency solar cells. The optimum cadmium content can be determined by balancing the improvements in grain size, optical energy gap, and charge transport characteristics. At x=1, the corresponding photovoltaic cell adopted the highest efficiency of 2.621%. In the future work, it is recommended to design tandem solar cells using thin CCZTS films as one of the absorber layers to improve the device efficiency.

Author Contributions: Hanaa I. Mohammed conceived and designed the research framework; Hanaa I.Mohammed and Eman M.Nasir carried out the experimental and computational work; Iqbal S. Naji provided critical guidance on the analytical methods and interpretation of results; Hanaa I.Mohammed performed the data analysis; Hanaa I. Mohammed prepared the initial draft of the manuscript. All authors have read and approved the final manuscript. All authors contributed to editorial changes in the manuscript. All authors have participated sufficiently in the work and agreed to be accountable for all aspects of the work.

Availability of Data and Materials: The datasets used and analyzed during the current study are available from the corresponding author on reasonable request.

Funding: This research received no external sources of funding.

Declaration of AI and AI-assisted Technologies in the Writing Process: AI tools were not used in drafting of the manuscript, production of images or graphical elements of the paper, or in the collection and analysis of data.

Conflict of Interest: The authors declare no conflict of interest.

References

1. Courel, M.; Nicolás, M. M.; Vigil-Galán, O. Study on the physical properties of Cu2ZnSnS4 thin films deposited by pneumatic spray pyrolysis technique. *Applied Chemical Engineering* 2021, 4(1), 9–14. https://doi.org/10.24294/ace.v4i1.652

2. Deokate, R. J.; Adsool, A. D.; Shinde, N. S.; Pawar, S. M.; Lokhande, C. D. Structural and optical properties of spray-deposited Cu2ZnSnS4 thin films. *Energy Procedia* 2014, 54, 627–633. https://doi.org/10.1016/j.egypro.2014.07.304

3. Ramanathan, K.; Teeter, G.; Keane, J. C.; Noufi, Y. R. Properties of high-efficiency CuInGaSe2 thin film solar cells. *Thin Solid Films* 2005, 480, 499–502. https://doi.org/10.1016/j.tsf.2004.11.050

4. Green, M. A. Consolidation of thin-film photovoltaic technology: the coming decade of opportunity. *Progress in Photovoltaics: Research and Applications* 2006, 14(5), 383–392. https://doi.org/10.1002/pip.702

5. Andersson, B. A. Materials availability for large-scale thin-film photovoltaics. *Progress in Photovoltaics: Research and Applications* 2000, 8(1), 61–76. https://doi.org/10.1002/(sici)1099-159x(200001/02)8:1<61::aid-pip301>3.0.co;2-6

6. Katagiri, H.; Saitoh, K.; Washio, T.; Shinohara, H.; Kurumadani, T.; Miyajima, S. Development of thin film solar cell based on Cu2ZnSnS4 thin films. *Solar Energy Materials and Solar Cells* 2001, 65(1-4), 141–148. https://doi.org/10.1016/S0927-0248(00)00088-X

7. Wadia, C.; Alivisatos, A. P.; Kammen, D. M. Materials availability expands the opportunity for large-scale photovoltaics deployment. *Environmental Science & Technology* 2009, 43(6), 2072–2077. https://doi.org/10.1021/es8019534

8. Green, M. A.; Emery, K.; Hishikawa, Y.; Warta, W.; Dunlop, E. D. Solar cell efficiency tables (version 42). *Progress in Photovoltaics* 2013, 21(5), 827–837. https://doi.org/10.1002/pip.2404

9. Kamoun, N.; Bouzouita, H.; Rezig, B. J. Fabrication and characterization of Cu2ZnSnS4 thin films deposited by spray pyrolysis technique. *Thin Solid Films* 2007, 515(15), 5949–5952. https://doi.org/10.1016/j.tsf.2006.12.144

10. Levcenco, S.; Dumcenco, D.; Wang, Y. P.; Huang, Y. S.; Ho, C. H.; Arushanov, E.; Tezlevan, V.; Tiong, K. K. Influence of anionic substitution on the electrolyte electroreflectance study of band edge transitions in single crystal Cu2ZnSn(SxSe1−x)4 solid solutions. *Optical Materials* 2012, 34(8), 1362–1365. https://doi.org/10.1016/j.optmat.2012.02.028

11. Yousefizad, M.; Golshan Bafghi, Z.; Shahriyari, A.; Javanmardi, A.; Hakimi Raad, N.; Ahmadi Shadmehri, A.; Samoodi, S.; Manavizadeh, N.; Moafi, A. Advancements in photovoltaic efficiency: The role of fluorine-doped CZTS in homojunction solar cells. *Heliyon* 2025, 11(3), e42300. https://doi.org/10.1016/j.heliyon.2025.e42300

12. Bakr, N. A.; Salman, S. A.; Hameed, S. A. Deposition and characterization of Cu2ZnSnS4 thin films for solar cell applications. *International Journal of Applied Engineering Research* 2018, 13, 3379–3388.

13. Seol, J. S.; Lee, S. Y.; Lee, J. C.; Nam, H. D.; Kim, K. H. Electrical and optical properties of Cu2ZnSnS4 thin films prepared by rf magnetron sputtering process. *Solar Energy Materials and Solar Cells* 2003, 75(1-2), 155–162. https://doi.org/10.1016/S0927-0248(02)00127-7

14. Walsh, A.; Chen, S.; Wei, S. H.; Gong, X. G. Kesterite thin-film solar cells: advances in materials modelling of Cu2ZnSnS4. *Advanced Energy Materials* 2012, 2(4), 400–409. https://doi.org/10.1002/aenm.201100630

15. Tanaka, T.; Nagatomo, T.; Kawasaki, D.; Nishio, M.; Guo, Q.; Wakahara, A.; Yoshida, A.; Ogawa, H. Preparation of Cu2ZnSnS4 thin films by hybrid sputtering. *Journal of Physics and Chemistry of Solids* 2005, 66(11), 1978–1981. https://doi.org/10.1016/j.jpcs.2005.09.037

16. Hall, S. R.; Szymanski, J. T.; Stewart, J. M. Kesterite, (Cu2)(Zn, Fe)SnS4, and stannite, (Cu2)(Fe, Zn)SnS4, structurally similar but distinct minerals. *The Canadian Mineralogist* 1978, 16(2), 131–137.

17. Schorr, S. J. Structural aspects of adamantine-like multinary chalcogenides. *Thin Solid Films* 2007, 515(15), 5985–5991. https://doi.org/10.1016/j.tsf.2006.12.100

18. Malerba, C.; Biccari, F.; Ricardo, C. L.; Valentini, M.; Chierchia, R.; Müller, M.; Santoni, A.; Esposito, E.; Mangiapane, P.; Scardi, P.; Mittiga, A. CZTS stoichiometry effects on the band gap energy. *Journal of Alloys and Compounds* 2014, 582, 528–534. https://doi.org/10.1016/j.jallcom.2013.07.199

19. Leow, S. W.; Li, W.; Tan, J. M. R.; Venkataraj, S.; Tunuguntla, V.; Zhang, M.; et al. Solution-processed semitransparent CZTS thin-film solar cells via cation substitution and rapid thermal annealing. *Solar RRL* 2021, 5(7), 2100131. https://doi.org/10.1002/solr.202100131

20. Jayakrishnan, R.; Raj, A.; Nair, V. G. Deposition of CZTS|ZnO hetero-junction using SILAR and spray pyrolysis. Semiconductors 2021, 55, 363–372. https://doi.org/10.1134/S106378262103009X

21. Ma, C.; Lu, X.; Xu, B.; Zhao, F.; An, X.; Li, B.; et al. Effect of CZTS/CdS interfaces deposited with sputtering and CBD methods on Voc deficit and efficiency of CZTS solar cells. *Journal of Alloys and Compounds* 2020, 817, 153329. https://doi.org/10.1016/j.jallcom.2019.153329

22. Boutebakh, F. Z.; Attaf, N.; Aida, M. S. Effect of growth temperature on the physical properties of kesterite Cu2ZnSnS4 (CZTS) thin films. *Discover Materials* 2025, 5, 4. https://doi.org/10.1007/s43939-025-00179-w

23. Peksu, E.; Karaagac, H. Characterization of Cu_2ZnSnS_4 thin films deposited by one-step thermal evaporation for a third generation solar cell. *Journal of Alloys and Compounds* 2021, 862, 158503. https://doi.org/10.1016/j.jallcom.2020.158503

24. Kumar, M.; Dubey, A.; Adhikari, N.; Venkatesan, S.; Qiao, Q. Strategic review of secondary phases, defects and defect-complexes in kesterite CZTS-Se solar cells. *Energy & Environmental Science* 2015, 8(11), 3134–3159. https://doi.org/10.1039/C5EE02153G

25. Almawgani, A. H. M.; Alzahrani, A.; Hajjiah, A.; Mehaney, A.; Elsayed, H. A.; Sayed, H. Optical absorption performance of CZTS/ZnO thin film solar cells comprising anti-reflecting coating of texturing configuration. *RSC Advances* 2023, 13(45), 31554–31568. https://doi.org/10.1039/D3RA05056D

26. Sivasankar, S. M.; Amorim, C. d. O.; Cunha, A. F. d. Progress in thin-film photovoltaics: a review of key strategies to enhance the efficiency of CIGS, CdTe, and CZTSSe solar cells. *Journal of Composites Science* 2025, 9(3), 143. https://doi.org/10.3390/jcs9030143

27. Duan, B.; Guo, L.; Yu, Q.; Shi, J.; Wu, H.; Luo, Y.; Li, D.; Wu, S.; Zheng, Z.; Meng, Q. Highly efficient solution-processed CZTSSe solar cells based on a convenient sodium-incorporated post-treatment method. *Journal of Energy Chemistry* 2020, 40, 196–203. https://doi.org/10.1016/j.jechem.2019.03.029

28. Tay, Y. F.; Hadke, S. S.; Zhang, M.; Lim, N.; Chiam, S. Y.; Wong, L. H. Improving the interfacial properties of CZTS photocathodes by Ag substitution. *Journal of Materials Chemistry A* 2020, 8(18), 8862–8867. https://doi.org/10.1039/d0ta02042g

29. Zhang, J.; Yang, Y.; Cui, G.; Alata, H.; Wang, Y.; Zhu, C. Enhancing electrical properties of Cu2ZnSn(S,Se)4 thin films via trace Co incorporation. *Materials Chemistry and Physics* 2021, 262, 124318. https://doi.org/10.1016/j.matchemphys.2021.124318

30. Bodnar, I. V.; Victorov, I. A.; Kalita, O. V.; Khoroshko, V. V.; Arushanov, E. Growth, crystal structure, and properties of Cu2Cd1−xZnxSnS4 solid solutions. *Solid State Sciences* 2021, 113, 106550. https://doi.org/10.1016/j.solidstatesciences.2021.106550

31. Hussein, H.; Yazdani, A. Investigation the influence of Fe(III) doping in Cu2ZnSnS4 semiconductor: structural, optical and magnetic properties. *Optik* 2019, 179, 505–513. https://doi.org/10.1016/j.ijleo.2018.10.138

32. Wang, W.; Liang, F.; Wang, J.; Guo, Y.; Qu, R.; Zhou, S.; Qiu, Y.; Sun, L. Enhanced performance of Cu2(CdxZn1−x)SnS4 thin film solar cells by optimizing Cd gradient distribution. *Materials Science in Semiconductor Processing* 2026, 205, 110365. https://doi.org/10.1016/j.mssp.2025.110365

33. Chennangod, S.; Ray, S.; Subrahmanya, A. P.; Tarafder, K.; Bhat, T. N. Temperature-dependent in situ Cd substitution at Zn sites in Cu2ZnSnS4 thin films via sol–gel method: Experimental and DFT insights. *Applied Surface Science* 2025, 712, 164166. https://doi.org/10.1016/j.apsusc.2025.164166

34. Su, Z.; Sun, K.; Han, Z.; Cui, H.; Liu, F.; Lai, Y.; Li, J.; Hao, X.; Liu, Y.; Green, M. A. Fabrication of Cu_2ZnSnS_4 solar cells with 5.1% efficiency via thermal decomposition and reaction using a non-toxic sol–gel route. *Journal of Materials Chemistry* A 2014, 2, 500–509. https://doi.org/10.1039/C3TA13533K

35. Su, Z.; Tan, J. M.; Li, X.; Zeng, X.; Batabyal, S. K.; Wong, L. H. Cation substitution of solution-processed Cu2ZnSnS4 thin film solar cell with over 9% efficiency. *Advanced Energy Materials* 2015, 5(19), 1500682. https://doi.org/10.1002/aenm.201500682

36. Su, Z.; Liang, G.; Fan, P.; Luo, J.; Zheng, Z.; Xie, Z.; Wang, W.; Chen, S.; Hu, J.; Wei, Y.; Yan, C. Device postannealing enabling over 12% efficient solution-processed Cu2ZnSnS4 solar cells with Cd2+ substitution. *Advanced Materials* 2020, 32(32), 2000121. https://doi.org/10.1002/adma.202000121

37. Wang, W.; Bai, H.; Zhi, G.; Zhao, Y.; Zhang, W.; Tang, Z. Preparation of Cu2CdxZn1−xSnS4 thin films by nanoparticle ink method. *Materials Research Express* 2021, 8(10), 106401. https://doi.org/10.1088/2053-1591/ac2d6c

38. Yan, C.; Sun, K.; Huang, J.; Johnston, S.; Liu, F.; Veettil, B. P.; Sun, K.; Pu, A.; Zhou, F.; Stride, J. A.; Green, M. A. Beyond 11% efficient sulfide kesterite $Cu_2Zn_{1-x}Cd_xSnS_4$ solar cell: effects of cadmium alloying. *ACS Energy Letters* 2017, 2(4), 930–936. https://doi.org/10.1021/acsenergylett.7b00129

39. Ghazwan, G. G.; Hussein, H. A.; Khudhur, A. H. Analytical modelling study of CZTS thin film solar cell for high efficiency performance. Revue des Composites et des Matériaux Avancés – *Journal of Composite and Advanced Materials* 2024, 34, 667–672. https://doi.org/10.18280/rcma.340515

40. Mazumder, S.; Mazumder, P.; Senthilkumar, K. Device modeling and study of AZO/i-ZnO/ZnS/CZTS-bilayer solar cell for different series and shunt resistances. *Solar Energy* 2022, 245, 46–57. https://doi.org/10.1016/j.solener.2022.08.055

41. Bouarissa, A.; Gueddim, A.; Bouarissa, N.; Maghraoui-Meherezi, H. Modeling of ZnO/MoS2/CZTS photovoltaic solar cell through window, buffer and absorber layers optimization. Materials Science and Engineering B 2021, 263, 114816. https://doi.org/10.1016/j.mseb.2020.114816

42. Wang, A.; Huang, J.; Cong, J.; Yuan, X.; He, M.; Li, J.; Yan, C.; Cui, X.; Song, N.; Zhou, S.; Green, M. A.; Sun, K.; Hao, X. Cd-free pure sulfide kesterite Cu2ZnSnS4 solar cell with over 800 mV open-circuit voltage enabled by phase evolution intervention. *Advanced Materials* 2024, 36(3), 2307733. https://doi.org/10.1002/adma.202307733

43. Tamin, M.; El Khouja, O.; Guemmaz, M.; Tamin, C.; Bocirnea, A. E.; Asshsahi, I.; Chaumont, D.; Galca, A. C. Towards a wide bandgap absorber: structural, morphological, and optical investigation of Ag-alloyed Cu2ZnSnS4 thin films. *Sustainable Energy & Fuels* 2025, 9(24), 6751–6760. https://doi.org/10.1039/d5se01303h

44. Gong, W.; Tabata, T.; Takei, K.; Morihama, M.; Maeda, T.; Wada, T. Crystallographic and optical properties of $(Cu,Ag)_2ZnSnS_4$ and $(Cu,Ag)_2ZnSnSe_4$ solid solutions. *Physica Status Solidi C* 2015, 12(6), 700–703. https://doi.org/10.1002/pssc.201400343

45. Mengü, I.; Muska, K.; Pilvet, M.; Mikli, V.; Dudutienė, E.; Kondrotas, R.; Krustok, J.; Kauk-Kuusik, M.; Grossberg-Kuusk, M. Comprehensive study of photoluminescence and device properties in Cu2Zn(Sn1−xGex)S4 monograins and monograin layer solar cells. *Solar Energy Materials and Solar Cells* 2024, 277, 113124. https://doi.org/10.1016/j.solmat.2024.113124

46. Yadav, S.; Chauhan, R. K.; Mishra, R. Simulation and optimization of CZTS/CZTSSe tandem photovoltaic cells for current balancing and efficiency improvement. *Renewable Energy* 2025, 255, 123810. https://doi.org/10.1016/j.renene.2025.123810

47. Ennouhi, N.; Aazou, S.; Er-Rafyg, A.; Laghfour, Z.; Sekkat, Z. Feasibility of exceeding 20% efficiency for kesterite/c-Silicon tandem solar cells using an alternative buffer layer: optical and electrical analysis. *Nanomaterials* 2024, 14(21), 1722. https://doi.org/10.3390/nano14211722

48. Callister, W. D.; Rethwisch, D. G. Materials science and engineering: An introduction; 10th ed.; Wiley: 2020.

49. Shewmon, P. Diffusion in solids; Springer: 2016.

50. Ohring, M. Materials science of thin films; 2nd ed.; Academic Press: 2002.

51. Mohammed, H. I.; Khdayer, I. H.; Naji, I. S. The effect of Ag content and heat treatment on structural and morphological properties of thin (Cu1−xAgx)2ZnSnSe4 films. *Chalcogenide Letters* 2020, 17(3), 107–115. https://doi.org/10.15251/cl.2020.173.107

52. Al-Maiyaly, B. K. H.; Abd Alrazak, A. H.; Mohammed, H. I.; Shaban, A. H. $HgBa_2Ca_{n-1}Cu_nO_{2n+2+\delta}$ superconducting thin films prepared by pulsed laser deposition. *Energy Procedia* 2017, 119, 490–500. https://doi.org/10.1016/j.egypro.2017.07.058

53. Migdadi, A. B.; Alzoubi, F. Y.; Al-Khateeb, H. M.; Alqadi, M. K. Structural and optoelectronic characterization of synthesized undoped CZTS and Cd-doped CZTS thin films. *Indian Journal of Pure & Applied Physics* 2022, 60, 138–149. https://doi.org/10.56042/ijpap.v60i2.54638

54. Athab, R. H.; Hussein, B. H. Preparation and study effect of vacuum annealing on structure and optical properties of $AgCuInSe_2$ thin film. *Digest Journal of Nanomaterials and Biostructures* 2022, 17, 1173–1180. https://doi.org/10.15251/DJNB.2022.174.1173

55. Ahmed, G. S.; Mohammed, H. I.; Akram, S.; Hassan, N.; Hassan, S. Effects of annealing time on physical properties of TiO_2 thin films prepared by RF magnetron sputtering technique. *2023 International Conference on Engineering Applied and Nano Sciences (ICEANS)*, 2023, pp. 1 – 6. IEEE Xplore. https://doi.org/10.1109/iceans58413.2023.10630468

56. Abdullah, H. I. Effect of annealing temperature and thickness on the structural and optical properties of CdSe thin films. *Ibn Al-Haitham Journal for Pure and Applied Science* 2017, 28, 43–53.

57. Mohammed, H. I. Synthesies and Study the Photovoltaic Properties of (Cu,Ag)2ZnSnS4/Si Solar Cell; PhD Thesis, College of Education for Pure Science, Ibn Al-Haitham, University of Baghdad, 2021.

58. Mohammed, H. I.; Khdayer, I. H.; Naji, I. S. Comparing the optical parameters for thin CAZTSe films prepared with various Ag ratios and annealing temperatures. In *AIP Conference Proceedings* 2021, 2372(1), 090005. AIP Publishing LLC. https://doi.org/10.1063/5.0068737

59. Pokpechi, K. U.; Asiegbu, A. D.; Oriaku, C. I.; Nwokorongwo, C. E.; Ugochukwu, J. Study of structural and optical properties of aluminum doped CoO (ACO) thin films. *IOSR Journal of Applied Physics* 2021, 13, 15–23. https://doi.org/0.9790/4861-1304011523

60. Schroder, D. K. Semiconductor Material and Device Characterization; Wiley: 2005. https://doi.org/10.1002/0471749095

61. Mohammed, H. I.; Ahmed, G. S.; Salman, S. H.; Abbas, I. A. IV characteristics of polycrystalline CAZTSe heterojunction solar cells at different Ag content and annealing temperatures. *International Journal of Nanoelectronics and Materials* 2023, 16(4), 749–758. https://doi.org/10.58915/ijneam.v16i3.1341

62. Benahmed, A.; Aissat, A.; Ayachi, B.; Sfina, N.; Saidi, F.; Vilcot, J. P. Efficiency improvement of thin film CuIn1−xGaxSe2 structure for solar cells applications. *Micro and Nanostructures* 2024, 188, 20780. https://doi.org/10.1016/j.micrna.2024.207801

63. Ibraheam, A. S.; Al-Douri, Y.; Hashim, U.; Ghezzar, M. R.; Addou, A.; Ahmed, W. K. Cadmium effect on optical properties of $Cu_2Zn_{1-x}Cd_xSnS_4$ quinternary alloys nanostructures. *Solar Energy* 2015, 114, 39–50. https://doi.org/10.1016/j.solener.2015.01.018

64. Rondiya, S. R.; Jadhav, Y. A.; Živković, A.; Jathar, S. B.; Rahane, G. K.; Cross, R. W.; et al. Solution-processed Cd-substituted CZTS nanocrystals for sensitized liquid junction solar cells. *Journal of Alloys and Compounds* 2022, 890, 161575. https://doi.org/10.1016/j.jallcom.2021.161575

65. Shannon, R. T.; Prewitt, C. T. Revised values of effective ionic radii. *Acta Crystallographica Section B* 1970, 26, 1046–1048. https://doi.org/10.1107/S0567740870003576

66. Rondiya, S. R.; Jadhav, Y.; Dzade, N. Y.; Ahammed, R.; Goswami, T.; De Sarkar, A.; Jadkar, S.; Haram, S.; Ghosh, H. N. Experimental and theoretical study into interface structure and band alignment of the Cu2Zn1−xCdxSnS4 heterointerface for photovoltaic applications. *ACS Applied Energy Materials* 2020, 3(6), 5153–5162. https://doi.org/10.1021/acsaem.9b02314

67. Abdo, S. K.; Rzaij, J. M. Copper molarity effect on the optical properties of Cu2CdSnS4 quaternary thin films. *Iraqi Journal of Science* 2021, 62(5), 1513–1523. https://doi.org/10.24996/ijs.2021.62.5.15

68. Park, H.; Hwang, Y. H.; Bae, B. S. Sol–gel processed Cu_2ZnSnS_4 thin films for a photovoltaic absorber layer without sulfurization. *Journal of Sol-Gel Science and Technology* 2013, 65, 23–27. https://doi.org/10.1007/s10971-012-2703-0

69. Ramizy, A.; Omar, K.; Hassan, Z.; Alattas, O. The effect of sub-band gap photon illumination on the properties of GaN layers grown on Si(111) by MBE. *Journal of Nanoparticle Research* 2011, 13, 7139–7148. https://doi.org/10.1007/s11051-011-0625-3

70. Kumar, A.; Tripathi, S. K. Enhanced room-temperature thermoelectric power factor of β-Zn_4Sb_3 thin films via surface roughness optimization. *Sustainable Energy & Fuels* 2025, 9(21), 5931. https://doi.org/10.1039/D5SE00688K

71. Nasir, E. M.; Alias, M. F.; Mohammed Ali, A. N. The influence of x ratio and annealing temperatures on structural and optical properties for $(CuO)_x(ZnO)_{1-x}$ composite thin films prepared by PLD. In *IOP Conference Series: Materials Science and Engineering* 2020, 757, 012053. IOP Publishing. https://doi.org/10.1088/1757-899X/757/1/012053

72. Sun, L.; Wang, W.; Hao, L.; Jia, Z.; Zhao, Y.; Zhi, G.; et al. Influence mechanism of Cd ion soaking on performance of flexible CZTSSe thin film solar cells. *Materials Science in Semiconductor Processing* 2022, 138, 106301. https://doi.org/10.1016/j.mssp.2021.106301

73. Tamin, C.; Chaumont, D.; Heintz, O.; Leray, A.; Adnane, M. Improvement of hetero-interface engineering by partial substitution of Zn in Cu_2ZnSnS_4-based solar cells. *EPJ Photovoltaics* 2022, 13, 24. https://doi.org/10.1051/epjpv/2022022

74. Kumar, Y. K.; Babu, G. S.; Chalapathi, U.; Kiran, Y. B.; Bhaskar, P. U.; Park, S. H. Growth and characterization of spray-deposited Cu2ZnSnS4 thin films by using two different carrier gases. *Physica B: Condensed Matter* 2023, 670, 415366. https://doi.org/10.1016/j.physb.2023.415366

75. Ahmed, H. J.; Kamil, A. A.; Habeeb, A. A.; Bakr, N. A. The influence of deposition temperature on the properties of chemically sprayed nanostructured Cu_2CdSnS_4 thin films. *International Research Journal of Science and Technology* 2020, 1(2), 149–155. https://doi.org/10.46378/irjst.2020.010211

76. Hassan, N. A.; Jaf, Z. N.; Salman, S. H.; Khudayer, I. H.; Ibrahem, H.; Miran, H. A. Influence of In-dopant on the optoelectronic properties of thermal evaporated $CuAlTe_2$ films. *Solid State Communications* 2023, 371, 115260. https://doi.org/10.1016/j.ssc.2023.115260

77. Ouni, B.; Boukhachem, A.; Dabbous, S.; Amlouk, A.; Boubaker, K.; Amlouk, M. Some transparent semi-conductor metal oxides: comparative investigations in terms of Wemple–DiDomenico parameters, mechanical performance and Amlouk–Boubaker opto-thermal expansivity. *Materials Science in Semiconductor Processing* 2010, 13(4), 281–287. https://doi.org/10.1016/j.mssp.2010.12.008

78. Henry, J.; Mohanraj, K.; Sivakumar, G. Vacuum evaporated FTO/$(Cu,Ag)_2ZnSnSe_4$ thin films and its electrochemical analysis. *Vacuum* 2019, 160, 347–354. https://doi.org/10.1016/j.vacuum.2018.11.055

79. Chen, S.; Gong, X. G.; Walsh, A.; Wei, S. H. Defect physics of the kesterite thin-film solar cell absorber Cu_2ZnSnS_4. *Applied Physics Letters* 2010, 96(2), 021902. https://doi.org/10.1063/1.3275796

80. Xiao, Z. Y.; Li, Y. F.; Yao, B.; Deng, R.; Ding, Z. H.; Wu, T.; et al. Bandgap engineering of $Cu_2Cd_xZn_{1-x}SnS_4$ alloy for photovoltaic applications: A complementary experimental and first-principles study. *Journal of Applied Physics* 2013, 114(18), 183107. https://doi.org/10.1063/1.4829457